Molecular Crystals and Liquid Crystals

Publication details, including instructions for authors and subscription information:
http://www.tandfonline.com/loi/gmcl20

Realization of POLICRYPS Gratings: Optical and Electro-Optical Properties

R. Caputo [a] , L. De Sio [a] , A. Veltri [a] , C. Umeton [a] & A. V. Sukhov [b]

[a] Liquid Crystal Laboratory - LICRYL, Centro di Eccellenza per Materiali Innovativi Funzionali in Calabria - CEMIF.CAL and Department of Physics - University of Calabria, Rende (CS), Italy

[b] Institute for Problems in Mechanics, Russian Academy of Science, Moscow, Russia

Version of record first published: 17 Oct 2011

To cite this article: R. Caputo, L. De Sio, A. Veltri, C. Umeton & A. V. Sukhov (2005): Realization of POLICRYPS Gratings: Optical and Electro-Optical Properties, Molecular Crystals and Liquid Crystals, 441:1, 111-129

To link to this article: http://dx.doi.org/10.1080/154214091009590

Mol. Cryst. Liq. Cryst., Vol. 441, pp. 111–129, 2005

ISSN: 1542-1406 print/1563-5287 online
DOI: 10.1080/154214091009590

Realization of POLICRYPS Gratings: Optical and Electro-Optical Properties

R. Caputo
L. De Sio
A. Veltri
C. Umeton
Liquid Crystal Laboratory – LICRYL, Centro di Eccellenza per Materiali Innovativi Funzionali in Calabria – CEMIF.CAL and Department of Physics – University of Calabria, Rende (CS), Italy

A. V. Sukhov
Institute for Problems in Mechanics, Russian Academy of Science, Moscow, Russia

In this paper we report a detailed characterization of a new structure (POLICRYPS) in which liquid crystal films are completely separated by polymer slices. This structure behaves as a Bragg diffraction grating and exhibits efficiencies that can become as high as 96–98%. The temperature dependence of the diffraction efficiency can be explained in terms of a Kogelnik-like model. A numerical simulation has been implemented which makes use only of real values of physical quantities and accounts for the experimental results with good accuracy. An applied electric field is able to switch off the grating, with a characteristic switching time which is lower than 1 ms. Threshold values of the field vary in the range 3–5 V/μm for gratings with a 1.39 μm fringe spacing.

Keywords: diffraction gratings; liquid crystals; optical switches; polymers

INTRODUCTION

Holographic switchable diffraction gratings are devices which can be used as basic components in a wide variety of telecommunication

This work has been accomplished within the INFM project PAIS 2000 and the Italian Government funded MURST projects PRIN 2000 and PRIN 2003.

Address correspondence to C. Umeton, Liquid Crystal Laboratory – LICRYL, Centro di Eccellenza per Materiali Innovativi Funzionali in Calabria – CEMIF.CAL and Department of Physics – University of Calabria, I-87036 Rende (CS), Italy. E-mail: umeton@fis.unical.it

systems, with the aim of realizing optical switching, wavelength routing, filtering spectral equalization, etc. The possibility of making electrically driven diffraction gratings based on Liquid Crystalline (LC) composite materials was first pointed out by Margerum and coworkers in late 80s [1,2]. The works of Sutherland *et al.* in early 90s [3,4] started the utilization of Polymer Dispersed Liquid Crystals (PDLC)-based gratings as new systems for obtaining electrically switchable diffraction and holographic devices. Later on, this kind of application became one of the main fields of interest in the area of PDLC based electro-optical devices [3–6]. The common goal of this kind of applications is to reach a high diffraction efficiency in gratings fabricated by simple and cheap processes. During the last decade, a lot of work has been carried out concerning the characterization of morphology and diffraction efficiency [7–9], as well as switching properties [10,11,5] of such devices. In order to obtain high diffraction efficiency and good optical quality gratings, it is necessary to achieve a sharp and uniform fringe morphology; many attempts have been made therefore in order to avoid those optical inhomogeneities (produced by nematic droplets) which have the same spatial scale as the wavelength of the diffracted radiation. PDLC gratings have been fabricated, in which the average nematic droplet size is quite small: resulting scattering losses are low (not exceeding some percent), while the diffraction efficiency becomes noticeably high, exceeding 90% for Bragg transmission gratings [12]. However, the value of the electric field, required to obtain a satisfactory switching effect, turns out to be not so low.

A different approach to avoid light scattering losses and limit the value of switching fields can be that of avoiding the formation of droplets at all, by creating uniform LC films alternated to slices of almost pure polymeric material. Recently an attempt has been made to fabricate a new kind of holographic gratings which exploit this morphology [13], and a new interesting device has been realized (we proposed to call it POLICRYPS, acronym of POlymer LIquid CRYstal Polymer Slices). In the following, a comparison between these new diffraction gratings and conventional PDLC systems is reported along with a first experimental characterization which shows the intrinsic advantages of the novel structure.

REALIZATION OF POLICRYPS DIFFRACTION GRATINGS AND COMPARISON WITH H-PDLC

The basic idea is to avoid the formation of a separate LC phase during the curing process [13]. In this way we avoid the growing of droplets, obtaining only a macroscopic phase separation, that is an almost

complete re-distribution of nematic and monomer components inside the sample. This result is obtained by exploiting the high diffusion which the nematic liquid crystal (NLC) molecules can undergo when they are in the isotropic state. The realization of POLICRYPS gratings is therefore the result of a new technique which includes the following steps:

a) The heating of a sample of photoinitiator – monomer – NLC mixture up to a temperature which is above the Nematic-Isotropic transition point of the NLC component;
b) The illumination of the sample with the interference pattern of a curing UV radiation;
c) The slow cooling of the sample below the Isotropic-Nematic transition point after the curing radiation has been switched off and the polymerization process has come to an end.

The obtained POLICRYPS structure presents a sharp morphology with polymer slices alternated to nematic films in which the director is parallel to the sample slabs and normal to the polymer slices. The origin of this orientation is actually under consideration: Probably, the diffusion process which takes place during the curing procedure is responsible of it.

In order to give a comparison between the performances of PDLC and POLICRYPS gratings, two samples cells have been prepared in which a PDLC and a POLICRYPS grating were realized from the same initial chemical mixture. The Set-up used for this experiment is the typical setup for the UV curing process and diffraction efficiency measurement [13]. The chemical mixture used to fill the cells has been prepared by diluting the NLC 5CB by Merck ($\approx$30 wt%) in the pre-polymer system Norland Optical Adhesive NOA-61; the sample cells, made by using indium tin oxide-(ITO)-coated glass slabs, were 16 μm thick. We have measured the first order diffraction efficiency at room temperature for both POLICRYPS and PDLC gratings, obtaining $\eta^{POLICRYPS} = 88\%$ and $\eta^{PDLC} = 41.2\%$. Although the value $\eta^{POLICRYPS}$ is quite high, it is not the highest that we have got; with different POLICRYPS gratings (not comparable with PDLC ones) we have reached values as high as 98%. The electro-optic response of the two gratings has been investigated by exploiting a low frequency (500 Hz) square wave voltage, and the results are reported in Figure 1. Figure 1(a) represents the switching curve of the POLICRYPS grating:

The behaviours of the first order transmittivity T_1 (circles), zero order transmittivity T_0 (squares) and total transmittivity T_{Tot} (triangles) are reported versus the applied electric field. Note that T_{Tot}

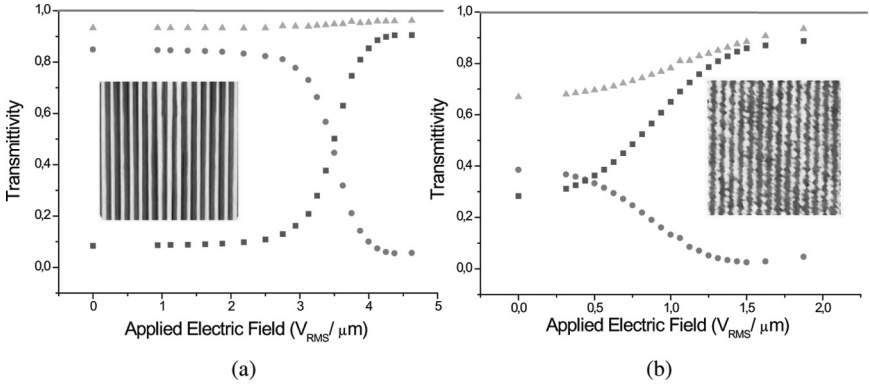

FIGURE 1 Applied field dependence of zero-order transmittivity T_0 (squares), first-order transmittivity T_1 (circles), and total transmittivity T_{Tot} (triangles) for (a) a POLICRYPS grating and (b) a PDLC grating at room temperature. Error bars are of the order of the symbol size. The insets show typical (a) POLICRYPS and (b) PDLC grating morphology with the same spatial period, observed under a polarizing optical microscope.

is only slightly less than 1 and remains approximately the same for all the values of the applied field. This indicates that the grating presents negligible scattering losses. The situation is quite different for the PDLC grating (Fig. 1(b)): the total transmittivity is well below 1 and increases as the applied voltage increases. We also note that, although the residual diffracted transmittivity of the POLICRYPS grating after the field is switched off is higher than that of the PLDC, the switching efficiency $h_{sw} \equiv \left(T_1^{on} - T_1^{off}\right)/T_1^{on}$ (where T_1^{on} and T_1^{off} are the first order transmittivity in the switch-on and switch-off conditions) is the same (93.3%) for both gratings. As far as switching voltages are concerned, the first diffracted beam is almost completely switched off by a field of about 1.5 V/μm, whereas a value of about 4.3 V/μm is needed to obtain the same effect in the POLICRYPS grating. This particular difference can be attributed to the average size of NLC droplets in the PDLC grating; evidently, they are large enough to make possible low switching fields.

DEPENDENCE OF THE DIFFRACTION EFFICIENCY ON TEMPERATURE

In the case of a thick diffraction grating, we can state, with good approximation, that only two waves are present in the system [14]:

the 0th diffracted order (reference wave) and the 1st diffracted order (signal wave). The diffraction efficiency (DE) is given, in this case, by the conventional Kogelnik formula:

$$\eta = \sin^2\left[\frac{\pi(\hat{e}_0 \cdot \hat{e}_1)(\varepsilon_1\varepsilon_{-1})^{1/2}L}{\varepsilon_0^{1/2}\lambda\cos\beta}\right] = \sin^2(\varphi(L,\lambda,T)) \qquad (1)$$

where $\hat{e}_0$ and $\hat{e}_1$ indicate the polarization unit vectors of probe and diffracted waves respectively, λ is the vacuum wavelength of the probe radiation, $\varepsilon_i (i = 1, 0, -1)$ stands for the i^{th} spatial Fourier component of the dielectric constant distribution across the fringe, β is the refraction angle of the probe beam inside the sample. Expression (1) represents an oscillating function of φ, with a periodic sequence of maxima and minima, which hold 1 and 0 respectively; the argument φ depends mainly on the sample thickness L and the probe wavelength λ_R. Although less evident, a dependence of φ on the sample temperature T also exists. Indeed, in holographic systems like these ones, the dielectric constants of polymer and liquid crystal components are generally chosen so that the polymer constant ε_p matches quite well the ordinary constant $\varepsilon_\perp$ of the liquid crystal. The extraordinary constant $\varepsilon_\parallel$ contributes, instead, to the modulation of the dielectric constant across the fringe. The temperature dependence of both values of the NLC dielectric constant, $\varepsilon_\parallel$ and $\varepsilon_\perp$ (taken from Ref. [15]), is presented in Figure 2 for the E7 NLC, along with the dependence of the polymer

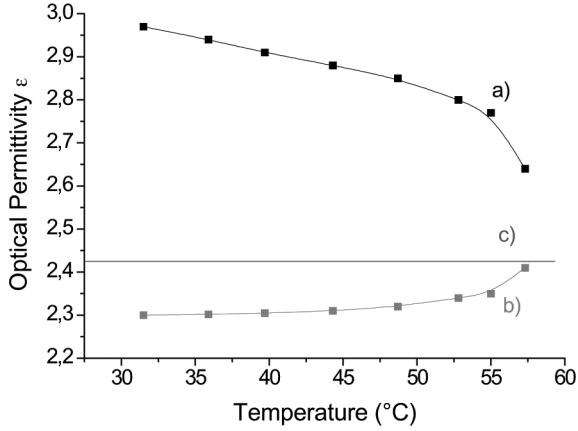

FIGURE 2 Temperature dependence of the dielectric constant of the pure components of the pre-syrup; a) $\varepsilon_\parallel$ for the E7 NLC; b) $\varepsilon_\perp$ for the E7 NLC; c) ε_p for the polymer.

one (Norland NOA-61, data supplied by the manufacturer). It is evident that the absolute value of the difference between each NLC dielectric constant and the polymer one decreases monotonously with the temperature increase. The Fourier coefficients ε_1 and ε_{-1}, are proportional to the modulation of the dielectric constant and are, therefore, dependent on temperature. Consequently, φ behaves as a monotonic decreasing function of temperature both for s and p polarizations of the probe beam. In the following an experimental analysis is reported.

EXPERIMENTAL CHARACTERIZATION OF THE DIFFRACTION EFFICIENCY

Sample cells used for this characterization were made by using ITO-coated glass slabs, with a thickness of $10\,\mu m$ set by suitable Mylar spacers. The initial mixture was prepared by diluting the Nematic Liquid Crystal BL-001 (conventional E7 NLC by Merck) in the prepolymer system NOA-61 (Norland Optical Adhesive). The NLC concentration was varied between $15\% \div 26\%$ in weight and several gratings were realized in this range. The curing of the gratings and their experimental analysis were performed using an optical set-up analogous to the one of ref. [13]. The particular technique which leads to the formation of the POLICRYPS morphology was applied to obtain the gratings and, in particular, samples were realized by heating and maintaining cells at 63°C before and during the curing process. This temperature is higher than the Nematic-Isotropic (NI) transition temperature of the pure E7 NLC (which is about 61°C). The curing process was performed by exposing, for about 1000 sec., the gratings to an UV ($\lambda_B = 0.351\,\mu m$) interference pattern (whose spatial period was $\Lambda = 1.34\,\mu m$) with a total intensity of $8\,mW/cm^2$. Finally, cells were cooled down to room temperature. A scanning electron microscope (SEM) picture of the sample with $C_N = 20\%$ is depicted in Figure 3.

In order to study the behavior of the diffraction efficiency as a function temperature [14], samples were placed in a hot stage and the temperature was monitored in the range 23–65°C. During the temperature variation, the diffraction efficiency η of gratings was measured by using a He-Ne laser ($\lambda_R = 0.6328\,\mu m$) probe beam of about $100\,\mu W$ power, slightly focused on the sample in order to obtain a spot diameter of about 1 mm; the angle of incidence of the probe beam was chosen for satisfying the Bragg condition. Transmitted and first order diffracted beams were detected, and the outputs were sent to both the data acquisition system and an oscilloscope for an immediate visualization of signals. In order to study the influence of an applied

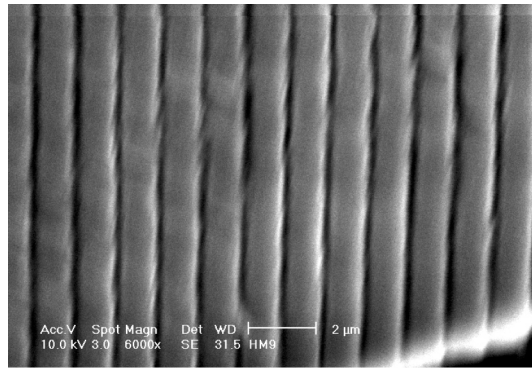

FIGURE 3 SEM picture of a typical POLICRYPS morphology; $C_N = 20\%$.

external voltage, we have applied to the samples, for several temperature values, a 1 kHz rectangular signal from a bipolar meander modulator (VC), with an amplitude which could be varied up to 200 V. A sketch of the diffraction geometry is presented in Figure 4. Here k_P and k_D indicate the wave-vectors of the probe and diffracted beams respectively.

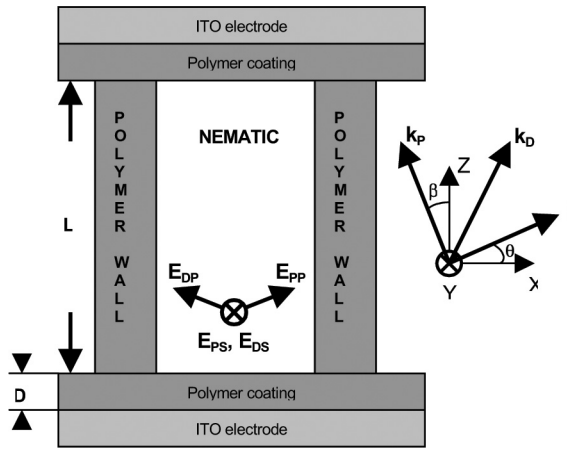

FIGURE 4 Sketch of the diffraction geometry. E_{PS}, E_{DS} are s polarized probe and 1st diffraction order electric field; E_{PP}, E_{DP} are p polarized ones; $k_{P,D}$ are probe and diffracted wave vectors; β - refraction angle; θ - alignment pre-tilt angle; $\hat{n}$ – NLC director; L – sample thickness; D – thickness of the polymer coating of ITO slabs.

The $\hat{n}$ vector represents the NLC director inside the sample. The angle θ takes into account the possibility that this director forms a tilt angle with the x axis. A preliminary result, common to all the experiments carried out, is that the polarization of the diffracted beam (see Fig. 4) always corresponds to the probe beam one.

Typical behaviors of diffraction efficiency versus temperature are presented in Figures 5, 6 for two different concentrations of the E7 NLC in the initial mixture and different cell thicknesses. The meaning of the black arrows in these figures will be explained in the following. It is evident that s and p polarized curves look quite different between each other. Furthermore, we note the following important features which are common to all the curves concerning both s and p polarized probe beams:

(i) curves always reach a steady state value for temperatures higher than 59°C, which corresponds to the NI transition temperature of the NLC in the sample (Fig. 2).
(ii) there is a minimum in the $\eta(T)$ curve of the s-probe, which occurs at the same temperature needed for the perpendicular permittivity $\varepsilon_\perp$ of the NLC to become equal to the polymer permittivity ε_P.
(iii) for the s probe beam, starting from room temperature we observe in $\eta(T)$ a monotonous decrease with temperature increase (Fig. 7).

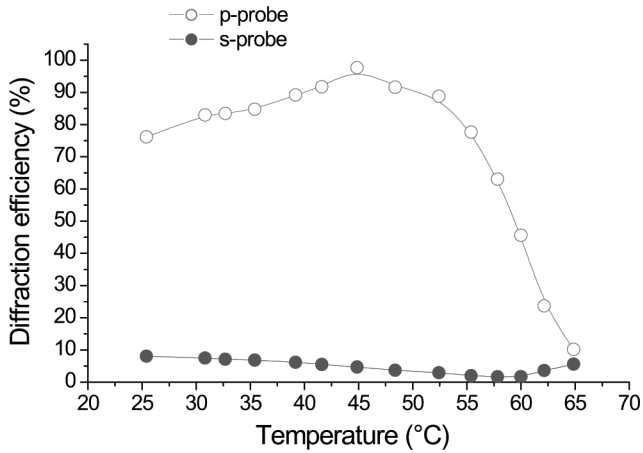

FIGURE 5 Temperature dependence of the diffraction efficiency for both s and p probe polarizations. $C_N = 15.0\%$; $L = 20\,\mu\text{m}$. Error bar is of the order of the dot size.

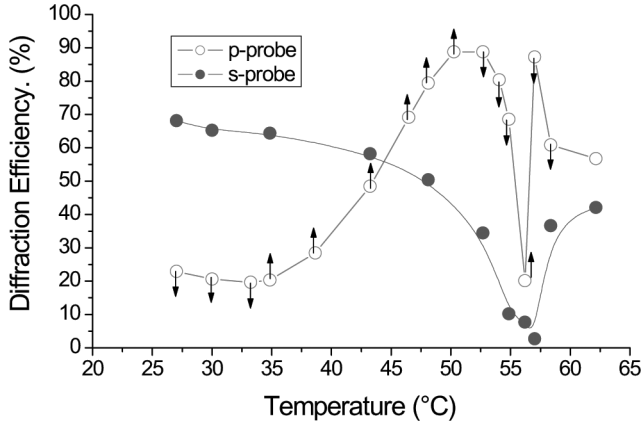

FIGURE 6 Temperature dependence of DE for both s and p probe polarizations; $C_N = 20{,}0\%$; $L = 9{,}7\,\mu m$. The direction of DE variation under an applied switching voltage is indicated by black arrows.

(iv) For high C_N values (Fig. 8) the $\eta(T)$ dependence for this beam passes through a maximum, a minimum and, probably, another maximum when going from the room to the NI transition temperature.
(v) If an external voltage is applied, the sign of the DE variation is defined by the local slope of the $\eta(T)$ curve.

Since Figures 5–8 concern samples which vary both in LC concentration and thickness, there is an experimental evidence that the optical properties of POLICRYPS gratings depend only on the actual

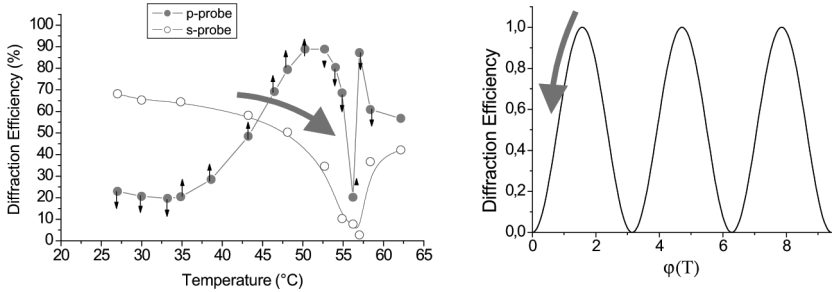

FIGURE 7 Going from room temperature to the NI transition temperature, there is a decrease of the s-probe diffraction efficiency, which starts from the first maximum and reaches the first minimum.

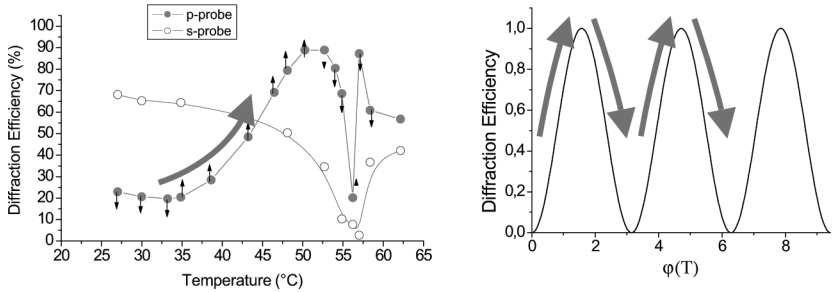

FIGURE 8 Going from room temperature to the NI transition temperature, the *p*-probe diffraction efficiency passes through a maximum, a minimum and then a second maximum.

value of the multi-variable argument φ of the Kogelnik function, independently of the way which has been followed to obtain that particular value.

There is, however, some discrepancy between experimental results and the theoretical ones predicted by (1). Maxima and minima values of the $\eta(T)$ curve given by (1) hold 1 and 0 respectively, while as a matter of fact, the corresponding experimental values are a little bit different. In our opinion this discrepancy can be due to some imperfection in the grating morphology. In particular, the nematic layer thickness within the fringe can vary slightly across the probe beam spot, thus leading to small variations in ε_1 and ε_{-1}. In this case, the experimentally observed $\eta(T)$ dependence does not correspond directly to expression (1), but to a superposition of several expressions of that kind, each having slightly different values of ε_1 and ε_{-1} in its argument. This fact leads to the observed non-unit maxima and non-zero minima. However, detailed considerations on such features require a more precise knowledge of the morphology of each particular grating, and we will go deeper insight this argument in the future.

A KOGELNIK-LIKE MODEL FOR POLICRYPS GRATINGS

We have implemented a theoretical approach which makes use of numerical simulations [18]. First of all, a simple estimation shows that, in our case the Bragg parameter holds $\rho = 2\lambda^2/\Lambda^2\varepsilon_1 \approx 11$, Λ being the grating fringe spacing, λ the probe wavelength and ε_1 the first order Fourier coefficient of the dielectric constant profile which represents the grating modulation. This value ensures that our POLICRYPS are thick diffraction gratings [16]. We also note that they are almost pure phase gratings, since no variation of the total transmitted

intensity (direct transmitted beam plus detectable diffraction orders) is observed with respect to the intensity of the probe beam transmitted before starting the curing process. In the case of a thick transmission diffraction grating with a fringe pattern perpendicular to the film surface we can write the following system of coupled wave equations [17]:

$$\begin{cases} \dfrac{\partial E_0}{\partial z} = ia(\hat{e}_0 \cdot \hat{e}_1)\varepsilon_{-1}E_1 \\ \dfrac{\partial E_1}{\partial z} = ia(\hat{e}_1 \cdot \hat{e}_0)\varepsilon_1 E_0 \end{cases} \tag{2}$$

where $a = \omega^2/2c^2k_z$ and E_0 and E_1 are the electric field amplitudes of the probe and diffracted waves respectively. This system of equations can be re-written in terms of the s and p polarization of the waves travelling in the grating: for the s polarization we can write the polarization unit vectors of probe and diffracted waves as $\hat{e}_0 = (0, 0, 1)$ and $\hat{e}_1 = (0, 0, 1)$. By substituting in (2) we obtain:

$$\begin{cases} \dfrac{\partial E_0^s}{\partial z} = ia\varepsilon_{-1}^0 E_1^s \\ \dfrac{\partial E_1^s}{\partial z} = ia\varepsilon_1^0 E_0^s \end{cases} \tag{3}$$

Where the p polarization is considered, $\hat{e}_0 = (\cos\beta,\ 0,\ \sin\beta)$ and $\hat{e}_1 = (\cos\beta,\ 0,\ -\sin\beta)$, therefore the equations are:

$$\begin{cases} \dfrac{\partial E_0^p}{\partial z} = ia\cos(2\beta)\varepsilon_{-1}^e E_1^p \\ \dfrac{\partial E_1^p}{\partial z} = ia\varepsilon_1^e E_0^p \end{cases} \tag{4}$$

In equations of systems (3) and (4), apexes "o" and "e" attributed to the Fourier components of permittivities denote that they are polarization-dependent. Solution of systems (3) and (4) yields:

$$\begin{aligned} \eta_s &= \left|\frac{E_1^s(z=L)}{E_{in}^s}\right|^2 = \sin^2\left[\frac{\pi\left(\varepsilon_1^o\varepsilon_{-1}^o\right)L}{\sqrt{\varepsilon_0^o}\lambda\cos\beta}\right] \\ \eta_p &= \left|\frac{E_1^p(z=L)}{E_{in}^p}\right|^2 = \sin^2\left[\frac{\pi\left(\varepsilon_1^e\varepsilon_{-1}^e\right)\cos(2\beta)L}{\sqrt{\varepsilon_0^e}\lambda\cos\beta}\right] \end{aligned} \tag{5}$$

Both solutions have a Kogelnik-like behaviour. Values of the permittivity components involved in (5) have to be estimated for each particular shape of the fringe profile. This shape can be supposed step-like, being composed of a uniform nematic film of relative thickness ξ $(0 < \xi < 1)$ with permittivity $\varepsilon_N^{o,e}$ and a slice of polymer of relative

thickness $(1-\xi)$, with ε_P permittivity value. The value of ξ can be assumed as equal to the volume concentration $C_{NV} \cong C_N$ of the nematic. The Fourier components of permittivity can be calculated analytically for this kind of profile and yield:

$$\begin{aligned} \varepsilon_{\pm 1}^{O,E} &= \pm \frac{i\left(\varepsilon_N^{O,E} - \varepsilon_P\right)}{2\pi} \left(\exp(\pm 2\pi i \xi) - 1\right) \\ \varepsilon_0^{O,E} &= \varepsilon_P + \left(\varepsilon_N^{O,E} - \varepsilon_P\right)\xi \end{aligned} \tag{6}$$

Substitution of these values into (5) gives:

$$\begin{aligned} \eta_s &= \sin^2\left[\frac{\left(\varepsilon_N^o - \varepsilon_p\right)\sin(\pi\xi)}{\sqrt{\varepsilon_p + \left(\varepsilon_N^o - \varepsilon_p\right)\xi}}\left(\frac{L}{\lambda\cos\beta}\right)\right] \\ \eta_p &= \sin^2\left[\frac{\left(\varepsilon_N^e - \varepsilon_p\right)\cos(2\beta)\sin(\pi\xi)}{\sqrt{\varepsilon_p + \left(\varepsilon_N^e - \varepsilon_p\right)\xi}}\left(\frac{L}{\lambda\cos\beta}\right)\right] \end{aligned} \tag{7}$$

Here $\varepsilon_N^o = \varepsilon_\perp$ while ε_N^e is given by the Fresnel equation

$$\varepsilon_N^{\mathrm{E}} = \left[\sin^2(\theta+\beta)/\varepsilon_\perp + \cos^2(\theta+\beta)/\varepsilon_\parallel\right]^{-1} \tag{8}$$

where θ is the director pre-tilt angle in the XZ plane (see Fig. 4).

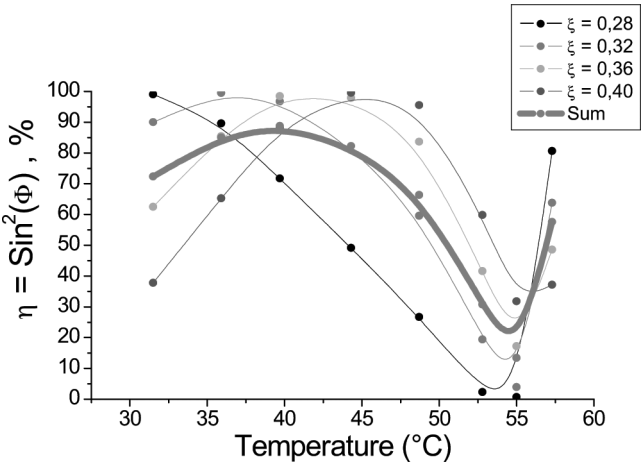

FIGURE 9 Calculated Kogelnik dependence of DE on temperature for several ξ values. The thick curve represents the average of all the other curves.

Introduction of the temperature dependence of $\varepsilon_{N,P}(T)$ (Fig. 2) into Equation (7), along with typical values of experimental parameters, gives the theoretical $\eta_{s,p}(T)$ curves for different values of ξ for a p polarized probe beam (Fig. 9). It is evident that the value of ξ dramatically influences the shape of these curves and the position and number of their extrema. The average curve (thick one) confirms our hypothesis that the behaviour of the diffraction efficiency is strongly influenced by the nematic layer thickness within the grating.

COMPARISON WITH EXPERIMENTAL RESULTS

A theoretical fit of the experimental curves is reported in Figure 10, where the utilized best fit value of ξ coincides with its expected value, that is the NLC concentration $\xi = C_N = 0.2$. This coincides also with the value deduced from the SEM photo (Fig. 3). In order to show the sensitivity of the fit to the particular ξ value, we have introduced in Figure 10 a theoretical curve obtained for the p probe with a slightly different (0, 18 instead of 0, 20) ξ value. As a result, the minimum is shifted down in temperature of 8°C.

Where the discrepancies observed in the extrema points of the p curve are concerned, we observe that, in fact, in these points the Kogelnik formula is no more valid and a further perturbation theory iteration is necessary in order to take into account the higher

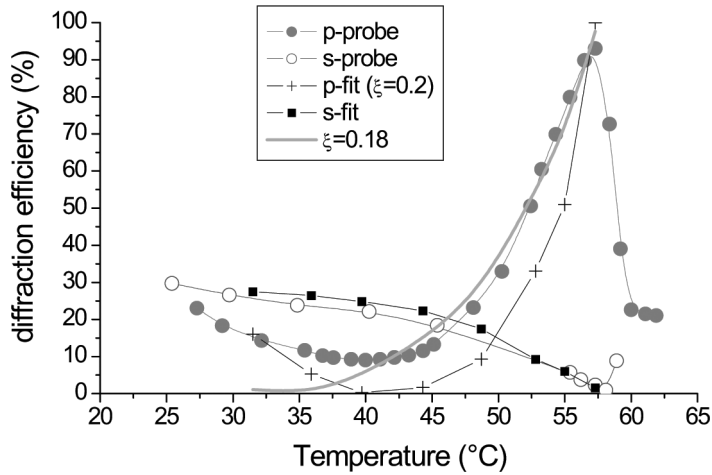

FIGURE 10 Theoretical fit of experimental curves of the DE dependence on temperature. The fit was made by putting $\xi = 0{,}2$ in expression (7). The continuous line refers to $\xi = 0{,}18$.

diffraction order contributions. The proper evaluation leads to a 2% diffraction efficiency for +2nd and −1st diffraction orders, that correspond well enough to the experimentally observed values. In its turn, a mean deviation of about 4% from extrema values 1 and 0 well fits the experimental results. Finally, by examining in details the morphology of the grating (see Fig. 3), it turns out that the width of the nematic films is not completely uniform across the grating: a typical scale of equal ξ length of the order of $d = 10\,\mu\text{m}$, can be recognize, wich corresponds to about 1% of the probe spot diameter. Therefore, it is more realistic to consider the DE of this grating written as a summation of several contributions:

$$\eta_{P,S}^{M} = \frac{1}{S}\sum_{n} \eta_{P,S}(\xi_n) S_n = \int_{-\infty}^{\infty} f(\xi)\eta_{P,S}(\xi)d\xi \tag{9}$$

Here S_n is the area of nth ξ-homogeneous spot with ξ_n value, S is the total probe cross section area, $f(\xi)$ represents the "ξ-area distribution function" normalized to S.

Assuming this function as a rectangle of $2\Delta\xi$ width centred at ξ_0, with $\Delta\xi/\xi_0 \ll 1$, the following expression for $\eta_{p,s}^{M}$ can be obtained:

$$\eta_{P,S}^{M} = \frac{1}{2\Delta\xi}\int_{\xi_0-\Delta\xi}^{\xi_0+\Delta\xi} \sin^2(v_{P,S}\sin(\pi\xi))d\xi \tag{10}$$

where:

$$v_P = \frac{\left(\varepsilon_N^E - \varepsilon_P\right)\cos(2\beta)}{\sqrt{\varepsilon_P + \left(\varepsilon_N^E - \varepsilon_P\right)\xi_0}}\left(\frac{L}{\lambda\cos\beta}\right)$$

$$v_S = \frac{\left(\varepsilon_N^O - \varepsilon_P\right)}{\sqrt{\varepsilon_P + \left(\varepsilon_N^O - \varepsilon_P\right)\xi_0}}\left(\frac{L}{\lambda\cos\beta}\right)$$

Neglecting the weak dependence on ξ of the square root in the denominator, we expand $\sin(\pi\xi)$ of expression (10) up to the linear term, and get the following result:

$$\eta_{P,S}^{M} = \sin^2\left(v_{P,S}\sin(\pi\xi_0)\right) + \frac{\cos\left(2v_{P,S}\sin(\pi\xi_0)\right)}{2} \times \left[1 - \frac{\sin\left(2\pi v_{P,S}\cos(\pi\xi_0)\Delta\xi\right)}{2\pi v_{P,S}\cos(\pi\xi_0)\Delta\xi}\right] \tag{11}$$

This expression reduces to (7) in the case $\Delta\xi = 0$, but for a non-zero value of $\Delta\xi$ it does not reach 0 and 1 extrema values. Results of fitting the same data of Figure 11 by Expression (11) are presented in Figure

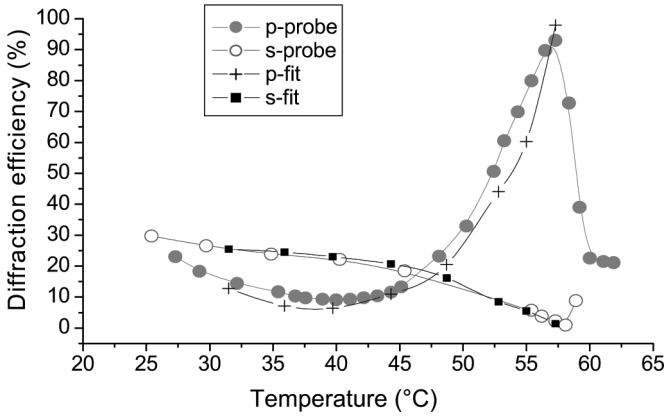

FIGURE 11 A more accurate fit of experimental curves of the DE dependence on temperature. The fit was made by putting $\xi = 0$, 2 in expression (11) and considering $\Delta\xi = 0$, 03.

11, where $\xi_0 = 0.2$ corresponds to C_N, and a best-fit value of $\Delta\xi = 0{,}03$ has been used.

SWITCHING EFFECTS

Where the diffraction efficiency dependence on an external electric field is considered, we can observe that for an amplitude value up to 13 V/μm, no modifications have been observed in the diffraction efficiency of the *s*-polarized probe beam; the circumstance confirms that this beam travels in the sample as an ordinary wave. For the *p* polarized probe beam, the value of the electric field required to produce a variation in the diffraction efficiency depends on the NLC concentration C_N, the typical field values (referred to as "switching threshold") varying in the range 1–5 V/μm.

Results for the applied field dependence of the diffraction efficiency of a *p* polarized probe beam are presented in Figure 12, for a nematic concentration $C_N = 26\%$. Curves show that, after the switching threshold is achieved, the sign of the diffraction efficiency variation depends on the actual value of the temperature. This sign is indeed indicated in Figures 6–8 by black "increase" and "decrease" arrows in correspondence of different temperature valves and it is easy to realize that they strictly correspond to the local sign of the curve slope. This means that the diffraction efficiency is increased by the applied field for slopes rising with temperature,

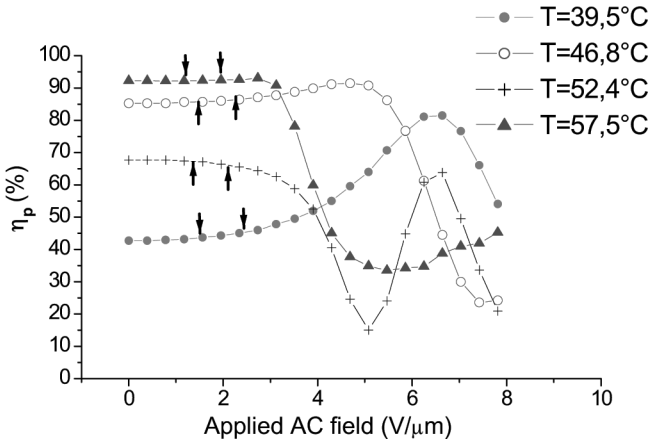

FIGURE 12 Dependencies of the DE of the p probe beam on the applied field for several temperature values; $C_N = 26.0\%$; $L = 12,\ 4\,\mu\text{m}$.

while it is decreased for descending slopes. From a theoretical point of view, we assume that the interaction of the NLC films between the fringes with external electric fields can be described in the framework of continuum theory. The threshold of Fredericksz transition in each nematic film, that is the "switching threshold", can be easily calculated using the standard variation technique [19] which yields:

$$E_{TH}^{\text{MIN}} = \frac{1}{(\xi_0 + \Delta\xi)\Lambda} U_F(T)$$

$$E_{TH}^{\text{MAX}} = \frac{1}{(\xi_0 - \Delta\xi)\Lambda} U_F(T) \tag{12}$$

$$U_F(T) = 2\pi\sqrt{\frac{\pi K_3(T)}{\Delta\varepsilon(T)}}$$

Here, U_F is the low-frequency threshold for pure nematic LC, K_3 is the bend Frank's constant (in our case the deformation is bend type) and $\Delta\varepsilon$ is the low frequency permittivity anisotropy of the NLC. Due to the range of values of the ξ parameter mentioned above, two limiting values of E_{TH} exist, denoting the fact that fringes with different thickness of the nematic film undergo Fredericksz transition at different field values. In Figure 12, the maximal and minimal values

of the threshold field calculated from (12) are depicted by arrows in the $\eta(E)$ curve. It can be seen that the points reasonably correspond to observed value of the switching threshold.

FUTURE DEVELOPMENTS

The features of POLICRYPS gratings give an intriguing possibility of realizing interesting application oriented developments. Work in this direction is already in progress and two main applications are actually under prototyping. A holographic tuneable beam splitter can be obtained by performing a substitution of the intersection part of two planar intersecting waveguides with a suitable POLICRYPS grating. The device can be easily engineered to fulfil the Bragg condition and maximize the diffraction efficiency of the grating. An optical beam entering the device can be splitted in two parts, the relative intensities of the obtained beams being controlled with continuity by an electro-optical control of the device.

A more sophisticate application of POLICRYPS gratings is given by a Bragg reflection filter. This is based on the concept of photonic band gap (PBG) which represents a window of the electromagnetic spectrum in which the propagation of light is forbidden. The presence of a PBG allows to engineer a particular filter which is able of reflecting only some wavelengths in a particular range of the incoming light. This kind of filter can be realized by introducing a POLICRYPS reflection grating between two consequent parts of a linear planar waveguide.

The character of innovation of this filter is represented again by the electro-optical control: The action of an external electric field can produce a tuning over a particular range of reflected wavelengths.

CONCLUSIONS

In conclusion, we have shown that, by utilizing a UV interference pattern and a suitable procedure, it is possible to realize a new structure in which polymer and NLC components are completely separated from each other, the NLC films being homogeneously aligned with the director perpendicular to the polymer slices. From the optical point of view, this structure represents a Bragg diffraction grating whose efficiency can be as high as 96–98%, exhibiting also a non-monotonic temperature dependence. This is due to the typical Kogelnik dependence of the DE of Bragg phase gratings upon the phase retardation modulation which, in our case, can easily achieve the value π in

10 μm thick samples. A Kogelnik-like model has been implemented which makes use only of real values of physical quantities (without necessity of introducing any fitting parameter) and accounts for the experimental results with good accuracy. Where the influence of an applied electric field is concerned, threshold values for switching the DE of POLICRYPS varies in the range 3–5 V/μm for gratings with a 1.39 μm fringe spacing. Comparison of these values with theoretical prediction reveals a good agreement, while the characteristic switching time, which is lower than 1ms, can be further reduced in the future by avoiding the formation of spurious polymer nets inside the nematic films.

REFERENCES

[1] Margerum, J. D., Lackner, A. M., Ramos, E., Smith, G. W., Vaz, N. A., Kohler, J. L., & Allison, C. R. "*Polymer dispersed liquid crystal film devices, and method of forming the same*", United States Patent #4,938,568 (1990, filed 1988).

[2] Margerum, J. D., Lackner, A.M., Ramos, E., Smith, G. W., Vaz, N. A., Kohler, J. L., & Allison, C. R. "*Polymer dispersed liquid crystal film devices*", United States Patent #5,096,282 (1992, filed 1990).

[3] Sutherland, R. L., Tondiglia, V. P., Natarajan, L. V., & Bunning, T. J. (1993). Bragg gratings in an acrylate polymer consisting of periodic polymer-dispersed liquid-crystal planes. *Chem. Mater.*, *5*, 1533.

[4] Sutherland, R. L., Tondiglia, V. P., Natarajan, L. V., Bunning, T. J., & Adams, W. W. (1994). Electrically switchable volume gratings in polymer-dispersed liquid-crystals. *Appl. Phys. Lett.*, *64*, 1074.

[5] Sutherland, R. L., Tondiglia, V. P., Natarajan, L. V., Bunning, T. J., & Adams, W. W. (1996). Electro-optical switching characteristics of volume holograms in polymer dispersed liquid crystals. *J. Nonl. Opt. Phys. & Materials*, *5*, 89.

[6] Sutherland, R. L., Tondiglia, V. P., Natarajan, L. V., Bunning, T. J., & Adams, W. W. (1995). Volume holographic image storage and electrooptical readout in a polymer-dispersed liquid-crystal film. *Opt. Lett.*, *20*, 1325.

[7] Jazbinsek, M., Olenik, I. D., Zgonik, M., Fontecchio, A. K., & Crawford, G. P. (2001). Characterization of holographic polymer dispersed liquid crystal transmission gratings. *J. Appl. Phys.*, *90*, 3831.

[8] Jazbinsek, M., Olenik, I. D., Zgonik, M., Fontecchio, A. K., & Crawford, G. P. (2002). Electro-optical properties of polymer dispersed liquid crystal transmission gratings. *M.C & L.C.*, *375*, 455.

[9] Duca, D., Sukhov, A. V., & Umeton, C. (1999). Detailed experimental investigation on recording of switchable diffraction gratings in polymer dispersed liquid crystal films by UV laser curing. *Liq. Crys.*, *26*, 931.

[10] Fuh, A. Y. G., Lee, C. R., & Ho, Y. H. (2002). Thermally and electrically switchable gratings based on polymer-ball-type polymer-dispersed liquid-crystal films. *Appl. Opt.*, *41*, 4585.

[11] Bowley, C. C., Kossyrev, P., Danworaphong, S., Colegrove, J., Kelly, J., Fiske, T., Yuan, H. J., & Crawford, G. P. (2001). Improving the voltage response of holographically formed polymer dispersed liquid crystals (H-PDLCs). *M.C & L.C.*, *359*, 647.

[12] Lucchetta, D. E., Karapinar, R., Manni, A., & Simoni, F. (2002). Phase-only modulation by nanosized polymer-dispersed liquid crystals. *J. Appl. Phys.*, *91*, 6060.

[13] Caputo, R., De Sio, L., Sukhov, A. V., Veltri, A., & Umeton, C. (2004). Realization of a new kind of switchable holographic grating made of liquid crystal films separated by slices of polymeric material. *Opt. Lett*., *29*, 1261–1263.
[14] Caputo, R., Veltri, A., Umeton, C. P., & Sukhov, A. V. (2004). Characterization of the diffraction efficiency of new holographic gratings with a nematic film-polymer-slice sequence structure. *J. Opt. Soc. Am. B*, *21*, 1939.
[15] Hallam, B. T., Brown, C. V., & Sambles, J. R. (1999). Quantification of the surface- and bulk-order parameters of a homogeneously aligned nematic liquid crystal using fully leaky guided modes. *J. Appl. Phys*., *86*, 6682–6689.
[16] Gaylord, T. K. & Moharam, M. G. (1981). Thin and thick gratings: terminology clarification. *Appl. Opt*., *20*, 3271.
[17] Shen, Y. R. (1984). *Principles of Nonlinear Optics*, John Wiley & Sons: New York.
[18] Caputo, R., Sukhov, A. V., Umeton, C., & Veltri, A. Characterization of the Diffraction Efficiency of New Holographic Gratings with a Nematic Film-Polymer Slice Sequence Structure (POLICRYPS). *J. Opt. Soc. Am. B* (to be published).
[19] de Gennes, P. J. (1974). *Physics of Liquid Crystals*, Oxford University Press: Oxford.